Journal of Computational Mathematics, Vol.22, No.2, 2004, 156–167.

NUMERICAL METHODS FOR MAXWELL'S EQUATIONS IN INHOMOGENEOUS MEDIA WITH MATERIAL INTERFACES *1)

Wei Cai
(*Department of Mathematics, University of North Carolina at Charlotte Charlotte, NC 28223, USA*)
(*E-mail: wcai@uncc.edu*)

Dedicated to Professor Zhong-ci Shi on the occasion of his 70th birthday

Abstract

In this paper, we will present some recent results on developing numerical methods for solving Maxwell's equations in inhomogeneous media with material interfaces. First, we will present a second order upwinding embedded boundary method - a Cartesian grid based finite difference method with special upwinding treatment near the material interfaces. Second, we will present a high order discontinuous spectral element with Dubinar orthogonal polynomials on triangles. Numerical results on electromagnetic scattering and photonic waveguide will be included.

Mathematics subject classification: 65M06, 65M60, 65M70, 78A45
Key words: Embedded Boundary Methods, Discontinuous Galerkin Method, Electromagnetic scattering photonic waveguides.

1. Introduction

Time domain solutions of Maxwell's equations have found applications in engineering problems such as designs of VLSI chips and photonic devices [1]. In contrast to frequency domain approaches where time harmonic Maxwell's equations are solved for given frequencies [2], the solutions from time domain simulation can produce a wide range of frequency information as well as transient phenomena required in many applications.

The most used time domain algorithm for Maxwell's equations is the simple Yee's finite difference scheme [3], which yields a second order approximation to the fields provided the underlying grids are rectangles and the conductor or dielectric boundaries are aligning with the mesh coordinates. Thus, the major disadvantage of the Yee's scheme is the limitation of the boundary or material interface geometry. To have second order accuracy, the scheme demands a locally conforming mesh to the boundary, as a result, tiny finite difference cells may limit the time step of the overall scheme.

Meanwhile, discontinuous Galerkin methods have attracted much research to handle the material interfaces in the media. Being higher order versions of traditional finite volume method [4], discontinuous Galerkin methods have been developed initially in 1970's for the study of neutron transport equations [5], and have now been applied to the area of computational fluid dynamics and the solution of Maxwell's equations [6] [7]. Discontinuous Galerkin methods inherit the flexibility of the finite element method in allowing unstructured meshes, and at the same time, employ high order polynomials for better accuracy and phase error in modelling wave propagations.

In this paper, we will first present a new upwinding embedded boundary method which employs a simple Cartesian grid to solve time dependent Maxwell's equations. The proposed

* Received January 31, 2004.
1) Supported of this work is provided by US National Science Foundation, Grant Number CCR-0098140.

embedded boundary method, like the immersed interface method (IIM) proposed to solve elliptic PDEs with discontinuous coefficients [8], uses a central difference scheme for mesh points away from the interfaces while modifications are made for grid points near the interfaces. Second, we will study a high order discontinuous spectral element with Dubinar orthogonal polynomials on triangles and Legendre orthogonal polynomials on quadrilaterals.

Numerical Results on electromagnetic scattering will be given for the upwinding embedded boundary methods while photonic waveguide with whispering gallery modes in microcylinders will be simulated with the discontinuous spectral element methods.

2. Upwinding Embedded Boundary Method

2.1. One Dimensional Scalar Model Equation

We will consider the following simple linear wave equation to demonstrate the basic idea of the upwinding embedded boundary method,

$$\frac{\partial u}{\partial t} + a\frac{\partial u}{\partial x} = 0, \qquad 0 \le x \le 1, \tag{2.1}$$

where the wave speed a is assumed to be positive and discontinuous at $x_d \in (0,1)$, and the solution $u(x,t)$ satisfies a jump condition at x_d,

$$r^+ u(x_d^+, .) - r^- u(x_d^-, .) = g. \tag{2.2}$$

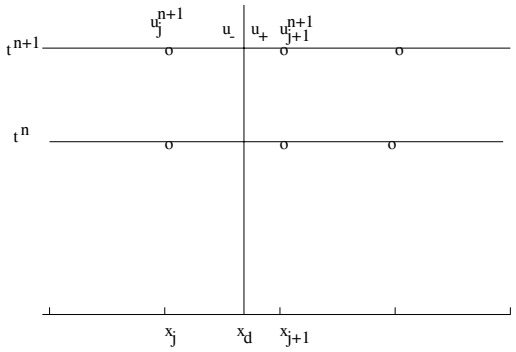

Figure 1: 1-D mesh with discontinuity at x_d

For a uniform grid $\{x_i = i\Delta x,\ 0 \le i \le N,\ \Delta x = \frac{1}{N}\}$, we have the numerical solutions u_i^n at grid points $(x_i,\ t^n), i = 0, 1, \cdots, N$, and also the solutions at both sides of the jump location x_d denoted as u_-^n, u_+^n (see Figure 1). Let us assume that $x_d \in [x_j, x_{j+1}]$,and $x_d = x_j + \alpha\Delta x$, $x_{j+1} - x_d = \beta\Delta x$, where $\alpha + \beta = 1$.

We will construct a uniformly second order finite difference method to solve (2.1) based on the Lax-Wendroff approach

$$u^{n+1} \doteq u^n + \Delta t u_t^n + \frac{(\Delta t)^2}{2}u_{tt}^n = u^n - a\Delta t u_x^n + \frac{(a\Delta t)^2}{2}u_{xx}^n, \tag{2.3}$$

where $\Delta t = CFL\frac{\Delta x}{|a|}$, and the spatial derivatives can be approximated by appropriate finite differences Let us assume that the solutions $u_i^n, 0 \le i \le N$, u_-^n and u_+^n have been obtained for the time step $t = t^n$. We will show how to obtain the solutions at the time step $t = t^{n+1}$.

- Solutions at the jump x_d

As the solution of (2.1) represents a wave propagating from left to right, we can thus use the PDE (2.1) to obtain u_-^{n+1} at the left side of x_d, namely

$$u_-^{n+1} = u_-^n - a^-\Delta t u_{x,-}^n + \frac{(a^-\Delta t)^2}{2} u_{xx,-}^n, \tag{2.4}$$

where the derivatives $u_{x,-}^n$ and $u_{xx,-}^n$ can be approximated by one-sided difference formulas.

To obtain the solution at the other side of the jump, we can simply use the jump condition (2.2) and have

$$u_+^{n+1} = \frac{1}{r^+}(g + r^- u_-^{n+1}). \tag{2.5}$$

- Solutions u_j^{n+1} and u_{j+1}^{n+1}

Solution u_j^{n+1} can also be obtained by an upwinding finite difference. In order to obtain u_{j+1}^{n+1}, we will use the solution u_+^{n+1} just obtained in (2.5), u_+^n, and $u_{j+1+k}^n, k \geq 1$. By examining the domain of influence of the hyperbolic equation, we can see that the characteristic originating from the time-space location (x_d, t^n) will pass the location $(x_{j+1}, t^n + CFL\frac{\beta\Delta x}{|a|})$. Without the knowledge of u_+^{n+1}, we may only be able to time-march the solution at x_{j+1} with a time step $CFL\frac{\beta\Delta x}{|a|}$, which could be very small if β approaches to zero.

2.2. One Dimensional Systems

Let us consider the linear system of equations

$$\frac{\partial \mathbf{u}}{\partial t} + A\frac{\partial \mathbf{u}}{\partial x} = 0, \tag{2.6}$$

where $\mathbf{u}(x,t) = (u_1(x,t), \cdots, u_n(x,t))^\intercal$The matrix A has different formulas across the discontinuity x_d representing a material interface $A = \begin{cases} A^-, & x < x_d \\ A^+, & x > x_d \end{cases}$. The matrix A can be diagonalized as follows

$$A = P\Lambda P^{-1},$$

where $\Lambda = \text{diag}(\lambda_1, ..., \lambda_p, ..., \lambda_n)$, $\lambda_1, \cdots, \lambda_p \geq 0, \lambda_{p+1}, \cdots, \lambda_n < 0$, and p is assumed to be the same on both sides of the interface throughout the paper. Solution $\mathbf{u}(x,t)$ may be discontinuous across the interface x_d and its values on both sides of the interface are related by the following jump condition,

$$R^+\mathbf{u}_+ - R^-\mathbf{u}_- = \mathbf{g}, \tag{2.7}$$

which can be rewritten in terms of the characteristic variable $\mathbf{w} = P^{-1}\mathbf{u}$ as

$$Q^+\mathbf{w}_+ - Q^-\mathbf{w}_- = \mathbf{g}, \tag{2.8}$$

where $Q^+ = R^+P^+$ and $Q^- = R^-P^-$.

The characteristic variables satisfy decoupled scalar wave equations

$$\frac{\partial w_i}{\partial t} + \lambda_i\frac{\partial w_i}{\partial x} = 0, \qquad 0 \leq i \leq n, \tag{2.9}$$

where the λ_i's may have a jump discontinuity at x_d.

- Solutions at the jump x_d

We will apply the same strategy as in Section 2.1 to the system of equations on the characteristic variable $\mathbf{w}$. Let $\mathbf{w}_\pm = \begin{pmatrix} \mathbf{w}_\pm^1 \\ \mathbf{w}_\pm^2 \end{pmatrix}$ be the partition of $\mathbf{w}_\pm$ according to the signs of the

eigenvalues. Similar to the case of single scalar equation, we know that $\mathbf{w}_-^1 = (w_{1,-}, \cdots, w_{p,-})^\intercal$ can be solved by an upwinding scheme for the differential equation (2.9) as in (2.4). And, $\mathbf{w}_+^2 = (w_{p+1,+}, \cdots, w_{n,+})^\intercal$ can also be obtained by an upwinding scheme from (2.9).

Next, we will apply the jump conditions in characteristic variables to obtain the rest components of the characteristic variables on both sides of x_d. We first partition the matrices Q^+ and Q^- as

$$Q^\pm = \begin{bmatrix} Q_{11}^\pm & Q_{12}^\pm \\ Q_{21}^\pm & Q_{22}^\pm \end{bmatrix}. \tag{2.10}$$

Then, from the jump condition (2.8), we can obtain $\begin{pmatrix} \mathbf{w}_+^1 \\ \mathbf{w}_-^2 \end{pmatrix}$ from the following system of equations

$$\begin{bmatrix} Q_{11}^+ & Q_{12}^- \\ Q_{21}^+ & Q_{22}^- \end{bmatrix} \begin{pmatrix} \mathbf{w}_+^1 \\ \mathbf{w}_-^2 \end{pmatrix} = \widetilde{\mathbf{g}}, \tag{2.11}$$

where $\widetilde{\mathbf{g}} = \mathbf{g} - \begin{bmatrix} Q_{11}^- & Q_{12}^+ \\ Q_{21}^- & Q_{22}^+ \end{bmatrix} \begin{pmatrix} \mathbf{w}_-^1 \\ \mathbf{w}_+^2 \end{pmatrix}$. The coefficient matrix above is invertible for well-posed hyperbolic systems.

Finally, we have the solution at $x_d, \mathbf{u}_\pm = P^\pm \mathbf{w}_\pm$.

- Solutions $\mathbf{u}_j^{n+1}$ and $\mathbf{u}_{j+1}^{n+1}$

We can obtain the solutions at x_j and x_{j+1} in the same way as in the case of one scalar equation by working with the decoupled scalar wave equations (2.9) for the characteristic variables.

2.3. Numerical Results - Scattering of a dielectric cylinder

We will consider a typical electromagnetic scattering problem, i.e. scattering by a dielectric cylinder in free space with a TM wave excitation. The cylinder is assumed to have a radius of $r_0 = 0.6$. If we assume that the cylinder is illuminated by a time-harmonic incident plane unit wavelength wave of the form

$$E_{\text{inc}}^z = e^{-i(k_1 x - \omega t)}, \qquad H_{\text{inc}}^y = -e^{-i(k_1 x - \omega t)},$$

where the propagation constant for homogeneous, isotropic free-space medium is $k_1 = \omega\sqrt{\mu_1 \epsilon_1}$, $\omega = 2\pi$, then the problem has an exact solution given in [1]

We consider a situation in which $\mu_1 = \epsilon_1 = 1$, i.e., the material exterior to the cylinder is assumed to be vacuum. We set $\epsilon_2 = 2.25$,$\mu_2 = 2$. In this case, E^z is continuous across the interface, but H^x, H^y and derivatives of H^x, H^y and E^z are all discontinuous. Figure 2 shows the contours and slices of the three computed field components at the time $t = 1.0$.

3. Discontinuous Spectral Element Method (DSEM) for Maxwell's Equations

The Maxwell's equations in a two dimensional domain $(x, y) \in \Omega$ can be written in a conservation form as

$$\frac{\partial \mathbf{Q}}{\partial t} + \nabla \cdot \mathbf{F}(\mathbf{Q}) = \mathbf{S}, \tag{3.1}$$

where the flux

$$\mathbf{F}(\mathbf{Q}) = (\mathbf{F}_1(\mathbf{Q}),\ \mathbf{F}_2(\mathbf{Q})) = \mathbb{A}\mathbf{Q}, \tag{3.2}$$

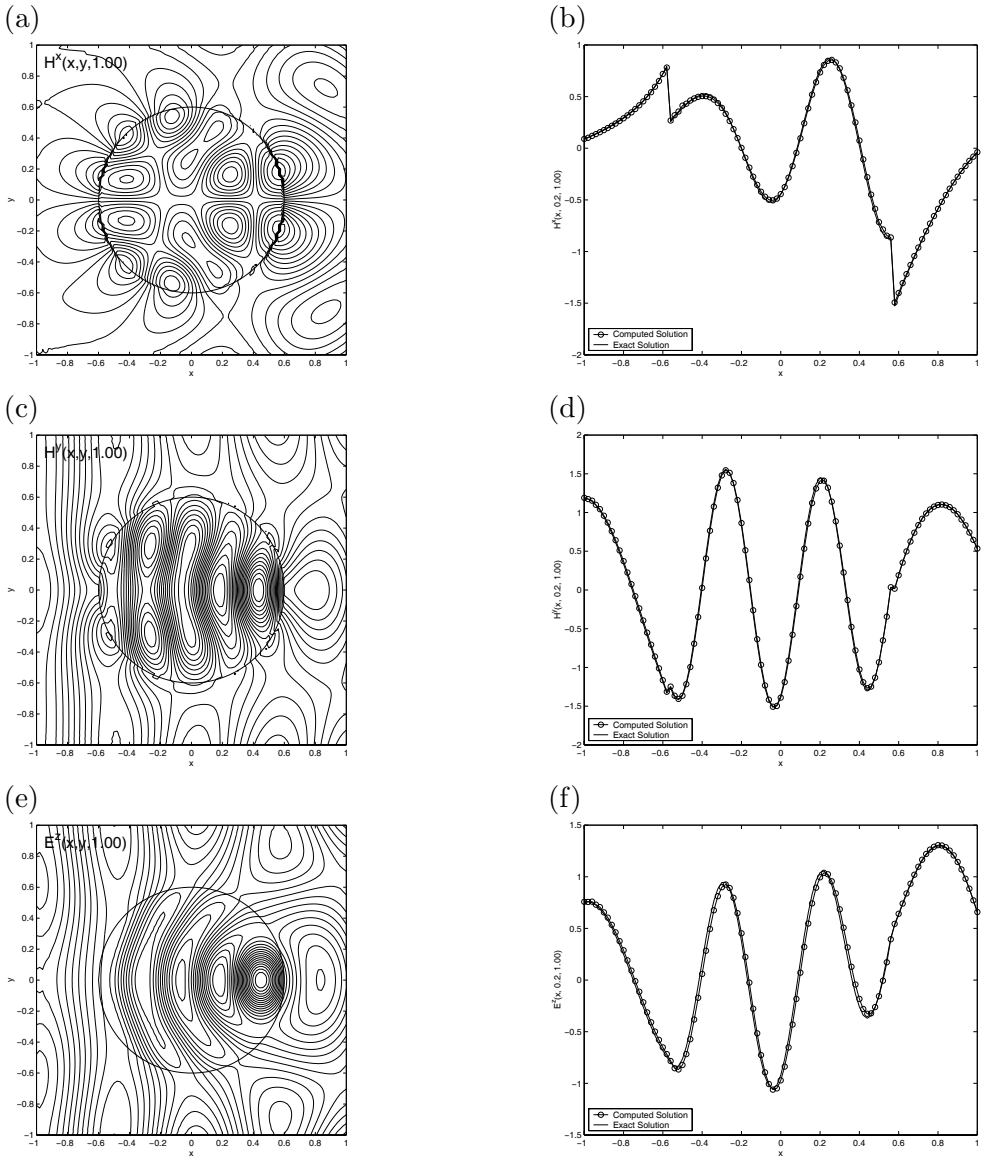

Figure 2: Scattering of a 2-D dielectric cylinder with material parameters $\mu_1 = \epsilon_1 = 1, \mu_2 = 2$ and $\epsilon_2 = 2.25$. On the left are contours of the computed solutions, and on the right are slices of the computed and the exact solutions. (a) $H^x(x, y, t = 1.0)$; (b) $H^x(x, 0.2, t = 1.0)$; (c) $H^y(x, y, t = 1.0)$; (d) $H^y(x, 0.2, t = 1.0)$; (e) $E^z(x, y, t = 1.0)$; and (f) $E^z(x, 0.2, t = 1.0)$.

and $\mathbb{A} = (A(\epsilon_r, \mu_r), B(\epsilon_r, \mu_r))$ will be given in (3.34) below.

To solve (3.1) in general geometries, the physical domain Ω under consideration is divided into non-overlapping quadrilateral and/or triangular elements, denoted by K. Each physical element K is mapped onto a reference element I, either a reference square or a reference triangle, by an isoparametric transformation.

We will name the coordinates in the physical element K as $\mathbf{x} = (x, y)$, while the coordinates in the reference element I as $\xi = (\xi, \eta)$. The transformation mapping between K and I can be generally described by $\mathbf{x} = \chi(\xi) = (x(\xi, \eta), y(\xi, \eta))$, under which the equations (3.1) on each element become

$$\frac{\partial \hat{\mathbf{Q}}}{\partial t} + \nabla_\xi \cdot \hat{\mathbf{F}}(\hat{\mathbf{Q}}) = \hat{\mathbf{S}}. \tag{3.3}$$

The new variables in (3.3) are

$$\hat{\mathbf{Q}} = J\mathbf{Q}, \quad \hat{\mathbf{S}} = J\mathbf{S}, \quad \hat{\mathbf{F}}(\hat{\mathbf{Q}}) = (\hat{\mathbf{F}}_1(\hat{\mathbf{Q}}),\ \hat{\mathbf{F}}_2(\hat{\mathbf{Q}})), \tag{3.4}$$

where

$$\hat{\mathbf{F}}_1(\hat{\mathbf{Q}}) = (y_\eta, -x_\eta) \cdot \mathbf{F}(\mathbf{Q}) = \frac{(y_\eta, -x_\eta)}{J} \cdot \mathbb{A}\hat{\mathbf{Q}}, \tag{3.5}$$

$$\hat{\mathbf{F}}_2(\hat{\mathbf{Q}}) = (-y_\xi, x_\xi) \cdot \mathbf{F}(\mathbf{Q}) = \frac{(-y_\xi, x_\xi)}{J} \cdot \mathbb{A}\hat{\mathbf{Q}}, \tag{3.6}$$

and J is the Jacobian of the transformation.

Let $\mathcal{T}_h$ be a triangularization with quadrilateral and/or triangular elements of the solution domain Ω. On each element $K \in \mathcal{T}_h$, ϵ_r and μ_r are assumed constant. We denote a finite dimensional space of smooth functions defined on the element K by $\mathcal{P}(K)$, which will be used to approximate the variable $\hat{\mathbf{Q}}$. For each element $K \in \mathcal{T}_h$, we set a finite element space V_h of test functions

$$V_h := \{v \in L^1(\Omega), \quad | \ v|_K \in \mathcal{P}(K), \quad \forall K \in \mathcal{T}_h\}. \tag{3.7}$$

In the discontinuous spectral element method, the solution $\hat{\mathbf{Q}} \in V_h^6$ is approximated by a linear combination of the basis functions (orthogonal polynomials if possible) on each element K, and the approximation is not required to be continuous across ∂K. First, we approximate the solution $\hat{\mathbf{Q}}$ element-by-element in terms of the basis functions $\psi_i(\xi, \eta), i = 1, 2, \cdots, N$.

$$\hat{\mathbf{Q}}(\xi, \eta, t) \approx \hat{\mathbf{Q}}_N(\xi, \eta, t) = \sum_{j=1}^{N} \hat{\mathbf{Q}}_j(t)\psi_j(\xi, \eta), \tag{3.8}$$

where $\hat{\mathbf{Q}}_i(t) \in R^6$ are the time dependent coefficients. For each $i = 1, 2, \cdots, N$, we require that

$$\int_I \left(\frac{\partial \hat{\mathbf{Q}}_N}{\partial t}\psi_i - \hat{\mathbf{S}}_N\psi_i - \hat{\mathbf{F}}_N \cdot \nabla\psi_i \right) \mathrm{d}\xi + \int_{\partial K} \mathbf{h}_K(\hat{\mathbf{Q}}_N^-, \hat{\mathbf{Q}}_N^+)\psi_i \mathrm{d}\mathbf{s} = 0, \tag{3.9}$$

where $\hat{\mathbf{Q}}_N^-$ is the approximate field value local to the element K, and $\hat{\mathbf{Q}}_N^+$ is the approximate value from the neighbor element, and $\mathbf{h}_K(\hat{\mathbf{Q}}_N^-, \hat{\mathbf{Q}}_N^+)$ is the numerical normal flux. The numerical normal fluxes $\mathbf{h}_K(\hat{\mathbf{Q}}_N^-, \hat{\mathbf{Q}}_N^+)$ can be obtained by solving a local Riemann problem. The Riemann problem for Maxwell's equations is discussed in detail in [13]. In the three space dimensions, the numerical normal fluxes for a dielectric interface or continuous medium can be written as

$$\mathbf{h}_K = \begin{bmatrix} \mathbf{n} \times \frac{(Y\mathbf{E} - \mathbf{n}\times\mathbf{H})^- + (Y\mathbf{E} + \mathbf{n}\times\mathbf{H})^+}{Y^- + Y^+} \\ \\ -\mathbf{n} \times \frac{(Z\mathbf{H} + \mathbf{n}\times\mathbf{E})^- + (Z\mathbf{H} - \mathbf{n}\times\mathbf{E})^+}{Z^- + Z^+} \end{bmatrix}. \tag{3.10}$$

where $Z = \sqrt{\frac{\mu}{\epsilon}}, Y = \frac{1}{Z}$.

3.1. Orthogonal Nodal Basis on Rectangles

We denote the space of polynomials of degree L or less by P_L. Let $\tau_i, \omega_i, i = 0, 1, \cdots, L$, be the Gauss points and weights in the interval [-1, 1]. Then a orthogonal basis for this space is the set of Lagrange interpolating polynomials, $\phi_i(\xi)$, with $i = 0, 1, \cdots, L$,

$$\phi_i(\xi) = \prod_{j=0, j\neq i}^{L} \frac{(\xi - \tau_j)}{(\tau_i - \tau_j)}. \tag{3.11}$$

On the standard reference square

$$Q_0 = [-1, 1] \times [-1, 1],$$

we define $P_{L,L} = P_L \times P_L$. The approximation basis functions of the scheme are

$$\psi_{mn}(\xi, \eta) = \phi_m(\xi)\phi_n(\eta), \quad 0 \leq m, n \leq L, \quad (\xi, \eta) \in Q_0, \tag{3.12}$$

and the grid points are

$$(\xi_m, \eta_n) = (\tau_m, \tau_n) \in Q_0, \quad 0 \leq m, n \leq L. \tag{3.13}$$

3.2. Dubiner Orthogonal Polynomial Basis on Triangles

The Dubiner basis [14] on triangles is obtained by transforming Jacobian polynomials defined on intervals to form polynomials on triangles. The n-th order Jacobian polynomials $P_n^{\alpha,\beta}(x)$ on $[-1, 1]$ are orthogonal polynomials under Jacobian weight $w(x) = (1 - x)^{\alpha}(1 + x)^{\beta}$.

To construct an orthogonal polynomial basis on the standard reference triangle

$$T_0 = \{(\xi, \eta) \mid \ 0 \leq \xi, \eta \leq 1, \ 0 \leq \xi + \eta \leq 1\}, \tag{3.14}$$

we consider the mapping between the reference square Q_0 and the reference triangle T_0,

$$\begin{cases} \xi &= \frac{(1+a)(1-b)}{4}, \\ \eta &= \frac{1+b}{2}, \end{cases} \quad \text{or} \quad \begin{cases} a &= \frac{2\xi}{1-\eta} - 1, \\ b &= 2\eta - 1. \end{cases} \tag{3.15}$$

The mappings in (3.15) basically collapse the top edge $b = 1$ of Q_0 into the top vertex (0,1) of T_0.

The Dubiner polynomial basis on T_0 is then defined as

$$\begin{aligned} g_{mn}(\xi, \eta) &= P_m^{0,0}(a)(1 - b)^m P_n^{2m+1,0}(b) \\ &= 2^m P_m^{0,0}\left(\frac{2\xi}{1-\eta} - 1\right)(1 - \eta)^m P_n^{2m+1,0}(2\eta - 1), \\ &0 \leq m, n, m + n \leq M. \end{aligned} \tag{3.16}$$

$\mathcal{P}_g = \{g_{mn}(\xi, \eta), \ 0 \leq m, n, m + n \leq M\}$ forms an orthogonal polynomial set, i.e.

$$(g_{mn}, g_{pq})_{T_0} = \frac{1}{8}\delta_{mp}\delta_{nq}, \tag{3.17}$$

and is complete in the polynomial space $\mathcal{P}_M$.

The finite element spaces over the reference triangle T_0 and the element K will be denoted as

$$\mathcal{P}(T_0) = \text{span}\{g_{mn}(\xi, \eta), \ 0 \leq m, n, m + n \leq M\}, \tag{3.18}$$

and

$$\mathcal{P}(K) = \text{span}\{g_{mn}(x, y) = g_{mn}(\xi, \eta), \ 0 \leq m, n, m + n \leq M\}, \tag{3.19}$$

respectively, and $\dim(\mathcal{P}(T_0)) = \dim(\mathcal{P}(K)) = (M + 1)(M + 2)/2$ and $\mathbf{x} = (x, y) = (x(\xi, \eta), y(\xi, \eta))$.

3.3. Numerical Result - Coupled Resonator Optical Waveguide (CROW)

As a numerical application, we will study CROW devices of coupled microcylinders where the optical energy transport is provided by the weak coupling of evanescent whispering gallery modes in the individual microcylinders [10].The whispering gallery modes (WGM) are electromagnetic resonances travelling in a dielectric medium of circular symmetric structures such as circular rods, microdisks and microspheres [11][12]. CROW devices have been considered for application of optical buffering, i.e. slowing down speed of lights for buffering purpose. In this type of application, propagation speed, arrival time and phase of the signals are critical parameters to have. A high order and phase-preserving numerical technique such as the DSEM is crucial. We will apply the proposed discontinuous spectral element method (DSEM) for Maxwell's equations to simulate the light propagation in photonic waveguides of coupled microcylinders.

3.3.1. Basics of Whispering Gallery Modes

Consider a circular dielectric cylinder of radius a and infinite length with dielectric constant ϵ_1 and magnetic permeability μ_1, which is embedded in an infinite homogeneous medium of material parameters ϵ_2 and μ_2. The fields may be derived entirely from the axial components of the electric and magnetic fields. With respect to a cylindrical coordinate system (r, θ, z), for a time factor $e^{-i\omega t}$, these axial components are solutions of Helmholtz equations $(\nabla^2 + k_1^2)\psi = 0$ for $r < a$, and $(\nabla^2 + k_2^2)\psi = 0$ for $r > a$, where ψ is either E_z or H_z. And $k_1 = \omega\sqrt{\epsilon_1\mu_1}$ and $k_2 = \omega\sqrt{\epsilon_2\mu_2}$ are the propagation constants inside and outside the cylinder, respectively. The fields must be finite at the center and, consequently, the wave functions within the cylinder will be represented by Bessel functions of the first kind J_n. Outside the cylinder Hankel functions of the first kind $H_n^{(1)}$ ensure the Sommerfeld outgoing conditions at the infinity. Therefore, solutions are of the type

$$\psi = e^{in\theta + ihz - i\omega t} \begin{cases} J_n(\lambda_1 r), & r < a, \\ H_n^{(1)}(\lambda_2 r), & r > a, \end{cases} \tag{3.20}$$

where h is the axial propagation constant, and

$$\lambda_1^2 = k_1^2 - h^2, \qquad \lambda_2^2 = k_2^2 - h^2.$$

Representing the field components E_z and H_z in terms of solutions in (3.20), and then applying Maxwell's equations, we can have the fields at all interior points [15], $r < a$,

$$H_r^i = \sum_{n=-\infty}^{\infty} \left[\frac{nk_1^2}{\mu_1\omega\lambda_1^2 r} J_n(\lambda_1 r)\ a_n^i + \frac{ih}{\lambda_1} J_n'(\lambda_1 r)\ b_n^i \right] F_n$$

$$E_r^i = \sum_{n=-\infty}^{\infty} \left[\frac{ih}{\lambda_1} J_n'(\lambda_1 r)\ a_n^i - \frac{\mu_1\omega n}{\lambda_1^2 r} J_n(\lambda_1 r)\ b_n^i \right] F_n \tag{3.21}$$

$$H_\theta^i = \sum_{n=-\infty}^{\infty} \left[\frac{ik_1^2}{\mu_1\omega\lambda_1} J_n'(\lambda_1 r)\ a_n^i - \frac{nh}{\lambda_1^2 r} J_n(\lambda_1 r)\ b_n^i \right] F_n \tag{3.22}$$

$$E_\theta^i = -\sum_{n=-\infty}^{\infty} \left[\frac{nh}{\lambda_1^2 r} J_n(\lambda_1 r)\ a_n^i + \frac{i\mu_1\omega}{\lambda_1} J_n'(\lambda_1 r)\ b_n^i \right] F_n \tag{3.23}$$

$$H_z^i = \sum_{n=-\infty}^{\infty} \left[J_n(\lambda_1 r)\ b_n^i \right] F_n,$$

$$E_z^i = \sum_{n=-\infty}^{\infty} \left[J_n(\lambda_1 r)\ a_n^i \right] F_n. \tag{3.24}$$

And at all exterior points, $r > a$, we have

$$H_r^e = \sum_{n=-\infty}^{\infty} \left[\frac{nk_2^2}{\mu_2 \omega \lambda_2^2 r} H_n^{(1)}(\lambda_2 r)\ a_n^e + \frac{ih}{\lambda_2} H_n^{(1)'}(\lambda_2 r)\ b_n^e \right] F_n$$

$$E_r^e = \sum_{n=-\infty}^{\infty} \left[\frac{ih}{\lambda_2} H_n^{(1)'}(\lambda_2 r)\ a_n^e - \frac{\mu_2 \omega n}{\lambda_2^2 r} H_n^{(1)}(\lambda_2 r)\ b_n^e \right] F_n \tag{3.25}$$

$$H_\theta^e = \sum_{n=-\infty}^{\infty} \left[\frac{ik_2^2}{\mu_2 \omega \lambda_2} H_n^{(1)'}(\lambda_2 r)\ a_n^e - \frac{nh}{\lambda_2^2 r} H_n^{(1)}(\lambda_2 r)\ b_n^e \right] F_n \tag{3.26}$$

$$E_\theta^e = -\sum_{n=-\infty}^{\infty} \left[\frac{nh}{\lambda_2^2 r} H_n^{(1)}(\lambda_2 r)\ a_n^e + \frac{i\mu_2 \omega}{\lambda_2} H_n^{(1)'}(\lambda_2 r)\ b_n^e \right] F_n \tag{3.27}$$

$$H_z^e = \sum_{n=-\infty}^{\infty} \left[H_n^{(1)}(\lambda_2 r)\ b_n^e \right] F_n,$$

$$E_z^e = \sum_{n=-\infty}^{\infty} \left[H_n^{(1)}(\lambda_2 r)\ a_n^e \right] F_n. \tag{3.28}$$

Here, the superscripts "i" and "e" represent "interior" and "exterior", respectively, and the prime denotes differentiation with respect to the argument $\lambda_1 r$ or $\lambda_2 r$, and

$$F_n = e^{in\theta + ihz - i\omega t}.$$

The coefficients of the expansions a_n^i, b_n^i, a_n^e, b_n^e, and the axial propagation constant h are determined by boundary conditions. At the cylindrical boundary $r = a$, the tangential components of the fields are continuous, yielding a 4×4 linear system for the coefficients for each n. In order to have nontrivial coefficients a_n^i, b_n^i, a_n^e, and b_n^e. the determinant of the 4×4 coefficient matrix should vanish, resulting in an algebraic equation for the axial propagation constant h [12]

$$\left[\frac{\mu_1}{u} \frac{J_n'(u)}{J_n(u)} - \frac{\mu_2}{v} \frac{H_n^{(1)'}(v)}{H_n^{(1)}(v)} \right] \left[\frac{k_1^2}{\mu_1 u} \frac{J_n'(u)}{J_n(u)} - \frac{k_2^2}{\mu_2 v} \frac{H_n^{(1)'}(v)}{H_n^{(1)}(v)} \right] = n^2 h^2 \left(\frac{1}{v^2} - \frac{1}{u^2} \right)^2, \tag{3.29}$$

whose roots are the allowed values of the propagation constant h and determine the characteristics or natural modes of propagation. These roots are discrete and form a twofold infinity, and for each n the denumerable infinity of roots are designated by $h_{n,m}$.

3.3.2. Maxwell's Equations for Coupled Microcylinders

For a WGM with the axial propagation constant h, the magnetic field $\mathbf{H} = (H_x, H_y, H_z)$ and the electric filed $\mathbf{E} = (E_x, E_y, E_z)$ in a rectangular coordinate system (x, y, z) may be expressed as

$$\mathbf{H}(x, y, z, t) = \mathbf{H}(x, y, t)\ e^{ihz}, \tag{3.30}$$

$$\mathbf{E}(x, y, z, t) = \mathbf{E}(x, y, t)\ e^{ihz}. \tag{3.31}$$

Substituting (3.30)(3.31) into Maxwell's equations

$$\mu\ \frac{\partial \mathbf{H}}{\partial t} = -\nabla \times \mathbf{E}, \tag{3.32}$$

$$\epsilon\ \frac{\partial \mathbf{E}}{\partial t} = \ \nabla \times \mathbf{H}. \tag{3.33}$$

we obtain the following scalar equations (in the MKS system of units), $\mathbf{Q} = (\mu \mathbf{H}, \epsilon \mathbf{E})^T$

$$\frac{\partial \mathbf{Q}}{\partial t}\ +\ A(\epsilon, \mu) \frac{\partial \mathbf{Q}}{\partial x}\ +\ B(\epsilon, \mu) \frac{\partial \mathbf{Q}}{\partial y}\ =\ \mathbf{S},$$

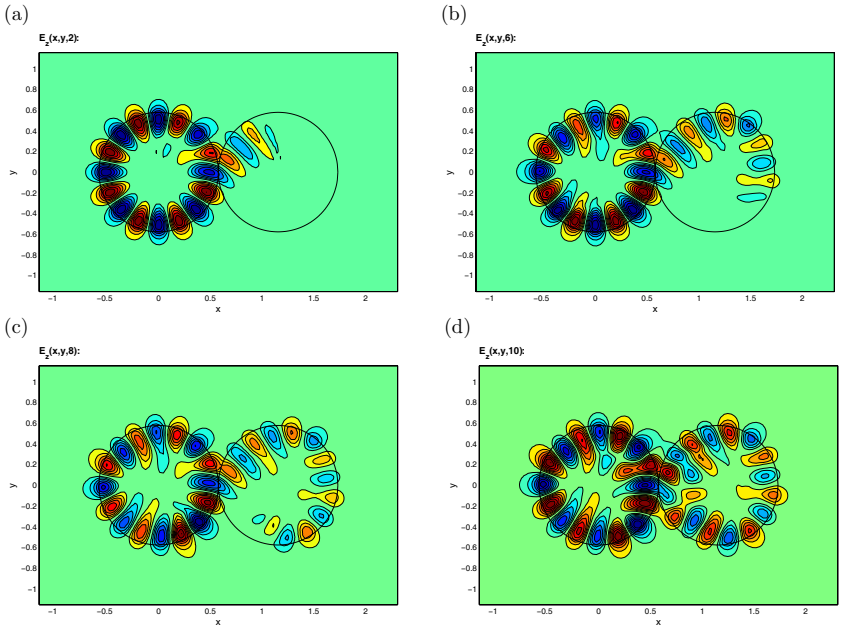

Figure 3: Optical energy transport by WGMs between two identical microcylinders in contact. The four sequential snapshots at $t = 2, 6, 8, 10$ (a)-(d) illustrate generation of a clockwise WGM in the right cylinder due to resonant optical coupling.

where

$$A(\epsilon,\mu) = \begin{bmatrix} 0 & 0 & 0 & 0 & 0 & 0 \\ 0 & 0 & 0 & 0 & 0 & -\frac{1}{\epsilon} \\ 0 & 0 & 0 & 0 & \frac{1}{\epsilon} & 0 \\ 0 & 0 & 0 & 0 & 0 & 0 \\ 0 & 0 & \frac{1}{\mu} & 0 & 0 & 0 \\ 0 & -\frac{1}{\mu} & 0 & 0 & 0 & 0 \end{bmatrix},$$

$$B(\epsilon,\mu) = \begin{bmatrix} 0 & 0 & 0 & 0 & 0 & \frac{1}{\epsilon} \\ 0 & 0 & 0 & 0 & 0 & 0 \\ 0 & 0 & 0 & -\frac{1}{\epsilon} & 0 & 0 \\ 0 & 0 & -\frac{1}{\mu} & 0 & 0 & 0 \\ 0 & 0 & 0 & 0 & 0 & 0 \\ \frac{1}{\mu} & 0 & 0 & 0 & 0 & 0 \end{bmatrix}, \qquad \mathbf{S} = \begin{bmatrix} ihE_y \\ -ihE_x \\ 0 \\ -ihH_y \\ ihH_x \\ 0 \end{bmatrix}. \tag{3.34}$$

3.3.3. Optical Coupling between Two Identical Cylinders in Contact

Two identical circular dielectric cylinders of infinite length in contact will be considered. The radiuses of the cylinders are $r_1 = r_2 = 0.5775$and material index $n = 3.2$, i.e. $\epsilon_1 = 10.24$ and $\mu_1 = 1$ inside both cylinders while the external medium is vacuum.

It can be shown that WGMs exist in such a cylinder. In fact, by setting the angular frequency $\omega = 2\pi$, and the azimuthal number $n = 8$, we find that the transcendental equation (3.29) has a solution $h = 6.80842739$ between $k_1 = 6.4\pi$ and $k_2 = 2\pi$. The WGM is denoted by $\text{WGM}_{8,0,0}$.

We will investigate the optical energy transport by WGMs from one cylinder to the other. To this end, we assume that initially there exists a WGM in the left cylinder and no fields exist inside the right cylinder. As initial conditions, the exact values of $\text{WGM}_{8,0,0}$ in the left cylinder

are taken in the entire computational domain except for the inside of the right cylinder, where a zero field is initialized.

To demonstrate the dynamics of the optical energy transport by WGMs from the left cylinder to the right cylinder, in Fig. 3 we show the snapshots of the E_z component at four different times. The initial state of the system is represented by a counterclockwise circulating wave, i.e. the fundamental mode $\mathrm{WGM}_{8,0,0}$, in the left cylinder. The four sequential snapshots Fig. 3(a)-(d) then illustrate the generation of a clockwise WGM in the right cylinder due to the optical coupling, and thus confirm the optical energy transport from the left cylinder to the right cylinder. The effect of the separation and size variation of the microcylinders on the optical transfer is studied in [16].

4. Conclusion

In this paper, we have presented two different methods in treating material interfaces for electromagnetic scattering in inhomogeneous media. The upwinding method is a Cartesian grid based method with second order accuracy, which avoids the accuracy degeneracy of the traditional Yee scheme near material interface. Further work is needed to extend the idea to 3-D problems and to higher order methods. The discontinuous spectral element method can give higher order accuracy for the solutions as long as the material interface is approximated by the underlying mesh accurately. In summary, the discontinuous spectral method has better accuracy than the upwinding embedded method for treating material interfaces at the expense of mesh generations.

References

[1] A. Taflove, Computational Electrodynamics - The Finite Difference Time-Domain Method, (Artech House, Boston, 1995).

[2] R.F. Harrington, Field Computation by Moment Methods, (Macmillian, New York, 1968).

[3] K.S. Yee, Numerical solution of initial boundary value problems involving Maxwell equations in isotropic media, *IEEE Trans. Antennas Propagate,* **14** (1966), 302.

[4] B. Cockburn and C.W. Shu, The local discontinuous Galerkin finite element method for convection-diffusion systems, *SIAM J. Numer. Anal.,* **35** (1998), 2440.

[5] P. LeSaint and P.A. Raviart, On a finite element method for solving the neutron transport equation, in Mathematical Aspects of Finite Elements in Partial Differential Equations, edited by C. De Boor Academic Press, New York, 1974, p.89.

[6] D. Kopriva, S.L. Woodruff, and M. Y. Hussaini, Discontinuous spectral element approximation of Maxwell's equations, in Discontinuous Galerkin Methods: Theory, Computation and Applications, edited by B. Cockburn, G. Karniadakis and C.-W. Shu, Springer-Verlag, New York, 2000, p.355.

[7] T. Warburton, Application of the discontinuous Galerkin method to Maxwell's equations using unstructured polymorphic hp-finite elements, in Discontinuous Galerkin Methods: Theory, Computation and Applications, edited by B. Cockburn, G. Karniadakis and C-W. Shu Springer-Verlag, New York, 2000, p.451.

[8] R.J. LeVeque and Z. Li, The immersed interface method for elliptic equations with discontinuous coefficients and singular sources, *SIAM J. Num. Anal.*, **31** (1994), 1019.

[9] C. Zhang and R.J. LeVeque, The immersed interface method for acoustic wave equations with discontinuous coefficients, *Wave Motion*, **25** (1997), 237.

[10] A. Yariv, Y. Xu, R.K. Lee and A. Scherer, Coupled-resonator optical waveguide: a proposal and analysis, *Opt. Lett.*, **24** (1999), 711.

[11] L. Rayleigh, Further applications of Bessel functions of high order to the whispering gallery and allied problems, *Phil. Mag.*, **27** (1914), 100.

[12] J.R. Wait, Electromagnetic whispering gallery modes in a dielectric rod, *Radio Science,* **2** (1967), 1005.

[13] A.H. Mahammadian, V. Shankar and W.F. Hall, Computation of electromagnetic scattering and radiation using a time-domain finite-volume discretization procedure, *Computer Physics Communications*, **8** (1991), 175.

[14] M. Dubiner, Spectral methods on triangles and other domains, *Journal of Scientific Computing,* **6** (1991), 345.

[15] J.A. Stratton, Electromagnetic Theory, McGraw-Hill, New York, 1941.

[16] S.Z. Deng, W. Cai, Discontinuous Spectral Element Methods for Optical Transfer by Whispering Gallery Modes in a Photonic Waveguide of Coupled Microcylinders, submitted to Journal of Computatioanal Physics, 2004.